

# Roles of Structural Disorder and Surface State in Photoluminescence of BaTiO<sub>3</sub> Nanoparticles

Nurul Norfarina Hasbullah<sup>1</sup>, Soo Kien Chen<sup>2</sup>, Kar Ban Tan<sup>3</sup>,  
Zainal Abidin Talib<sup>2</sup> and Oon Jew Lee<sup>1\*</sup>

<sup>1</sup>Advanced Nano Materials (ANoMa) Research Group, <sup>2</sup>School of Fundamental Science, Universiti Malaysia Terengganu, 21300 Kuala Terengganu, Terengganu, Malaysia

<sup>2</sup>Department of Physics and <sup>3</sup>Department of Chemistry, Faculty of Science, Universiti Putra Malaysia, 43400 Serdang, Selangor, Malaysia

\*Corresponding author (e-mail: oonjew@umt.edu.my)

This work provides an insight on the photoluminescent behaviour of BaTiO<sub>3</sub> (BTO) nanoparticles synthesised via a hydrothermal process at 200°C with further heat treatment at 1000°C. The morphology of BTO nanoparticles evolved to pseudo-ellipsoid by tuning the concentration ratio of barium precursors (Ba), oleic acid (OA) surfactant and tert-butylamine (TA) additive. Tunable optical band gaps (3.58–4.06 eV), Urbach tails in UV–Vis absorption spectra and the enhanced intensity of room temperature photoluminescence at violet wavelength (433.7 nm) were observed in BTO nanoparticles. The structural evolution and phase formation indicated that structural disorder and surface state share equal dominant factors for improving the photoluminescence at violet wavelength, tuning optical band gaps and exhibiting Urbach effect in the absorption spectra.

**Key words:** BaTiO<sub>3</sub>, ferroelectric, photoluminescence, Urbach tail

*Received: May 2019; Accepted: October 2019*

Barium titanate, BaTiO<sub>3</sub> (BTO) is a subject of continuing interest as a lead-free ferroelectric material which serves as an alternative to industrial standard ferroelectrics such as lead zirconate titanate Pb[Zr<sub>x</sub>Ti<sub>1-x</sub>]O<sub>3</sub>. BTO is a promising candidate used in diverse applications ranging from multilayer ceramic capacitors to photodetector [1, 2]. Researchers are devoted to fulfil the demand of miniaturized electronic devices by diminishing the size of BTO to nano-scale [3]. However, the functionalities of BTO-based nanostructures such as piezo-displacement, dielectric permittivity, dissipation factor and ferroelectric polarization are shaped-driven and size-dependent [4]. As the size of BTO decreases towards nano, progressing reductions in its functionalities are observed. Hence, the investigation of BTO nanoparticles is still plagued by trade-off problems between functionality and size effects, inhibiting their viability and flexibility as oxide-based electronics.

Although the investigation of BTO is prevalent on the ferroelectric-related functionality, the photoluminescent behaviour of BTO nanostructures has never waned. BTO is a complex photoluminescence pervoskite amenable to band gap tunings (2.8-3.47 eV) [5]. The consequent change in the crystal structure is anticipated to affect the photoluminescence response in BTO. The visible luminescent quenching effect of pure BTO crystals have been long mitigated beyond cryogenic temperatures as low as 45 K [6]. Intense visible photoluminescence at room temperature has been detected in amorphous BTO thin films and BTO

ultrafine particles owing to grain size and crystallite disorder [7-9]. The origin of the photoluminescence of BTO is not yet completely settled although a framework of photoluminescence mechanism of BTO has been outlined. Crystallite disorder, rare-earth doping, surface state and polarization influence provide some evidence to evaluate the origins of photoluminescence [10].

In this work, we provide an insight on the photoluminescent behaviour of BTO nanostructures synthesised via a hydrothermal process and heat treatment. Combining the aids from oleic acid surfactant and tert-butylamine additive, the morphology of BTO nanostructures evolved from nanocube to pseudo-ellipsoid [7, 11]. We demonstrated that structural disorder and surface state share equal dominant factors on BTO nanostructures for improving the photoluminescence at violet wavelength.

## EXPERIMENTAL SECTION

Barium hydroxide octahydrate, H<sub>2</sub>BaO<sub>2</sub>·8H<sub>2</sub>O was dissolved and added to titanium (IV) bis(ammonium lactato) dihydroxide, C<sub>6</sub>H<sub>18</sub>N<sub>2</sub>O<sub>8</sub>Ti with Ba/Ti ratio of 1. The solution was maintained at pH 12 with 5 M sodium hydroxide, NaOH before mixing with tert-butylamine (TA) and oleic acid (OA) under continuous stirring. The mixture molar ratios were fixed at (1:3:3) and (1:2:2) for Ba: TA: OA, and the resulting solutions were transferred into a Teflon lined stainless steel autoclave. The autoclave was sealed and

heated at 200°C for 72 hours in an oven. The as-synthesised BTO precipitates were obtained after several washes with ethanol. Subsequent calcinations in air were carried out on the as-synthesized BTO powders at 1000°C for 4 hours. These calcined BTOs were denoted as BTO-1000. The phase and crystal structure of the samples were characterized by X'Pert Pro PW3040 MDP/Panalytical X-ray diffractometer (XRD) using Cu-K<sub>α</sub> radiation source. The XRD data were collected from 20° to 80° with a step size of 0.033° and analyzed via the X'Pert HighScore Plus software. The thermal behaviour of the as-synthesised BTO was examined by thermogravimetric analyzer (TGA/ SPTA 851, Mettler Toledo) at the heating rate of 10°C min<sup>-1</sup>. The structural morphology of the BTOs was determined by field emission scanning electron microscopy (FESEM). The photoluminescence spectra of the BTOs were taken at room temperature using photoluminescence spectrophotometer the UV-3600/Shimadzu UV-Vis spectrometer while the optical absorption spectra were recorded by LS55 Perkin Elmer fluorescence spectrometer with excitation wavelength of 325 nm.

## RESULTS AND DISCUSSION

XRD patterns of the hydrothermal as-synthesized BTO and heat-treated BTO-1000 for different ratios of Ba: TA: OA, 1:2:2 and 1:3:3, are shown in Figure 1. The phase of the as-synthesized BTO (1:2:2) and (1:3:3) changed from amorphous to crystalline after calcination at 1000°C. There was no trace of barium carbonate, BaCO<sub>3</sub> phase in BTO-1000 (1:3:3) which evidenced that the BTO-1000 was in single phase. BaCO<sub>3</sub> was found in BTO-1000 (1:2:2) as the secondary phase that matched with ICSD 98-005-

8847. Both BTO-1000 (1:2:2) and (1:3:3) were indexed to BaTiO<sub>3</sub> with tetragonal crystal structure (ICSD 98-007-8876). The interceding of BaCO<sub>3</sub> phase was also reported previously [7, 12] due to the lack of Ti<sup>3+/4+</sup> in BTO (1:2:2). This allows Ba cations to interact with airborne CO<sub>2</sub> during the conversion of BaTiO<sub>3</sub>. It is suggested the BaCO<sub>3</sub> phase can be eliminated if the conversion reaction is conducted either in an inert atmosphere or vacuum [13]. Alternatively, the usage of CO<sub>2</sub>-free water as well as rinsing the precipitates with acetic acid help to remove the BaCO<sub>3</sub> phase [14].

The crystallization process of BTO via hydrothermal synthesis consisted of the formation of titanium hydroxyl and followed by a reaction between titanium hydroxyl and barium cations. By controlling the initial molar ratios of the precursors, surfactant and additive, the shape and size of BTO can be tailored to form nanocubes [3, 15]. Since the as-synthesized BTO (1:2:2) and BTO (1:3:3) were amorphous, the morphology of the particles are not discussed herein. BTO-1000 (1:2:2) and (1:3:3) did not possess cubic shape with ordered arrays as our previous studies [7, 12], whereas they appeared in an irregular pseudo-ellipsoid morphology with wide size distributions (as depicted in Figure 2). These pseudo-ellipsoids of BTO-1000 (1:2:2) and (1:3:3) tend to agglomerate and their average sizes were 81.9 nm and 109.3 nm, respectively. The cubic morphology of BTO as reported in our previous study [7] could not be synthesised successfully in these proportions due to low concentration of oleic acid and tert-butylamine [15]. Tert-butylamine plays an important role in tailoring the size of BTO while it stabilizes Ti hydroxyl and accelerates the growth of BTO.

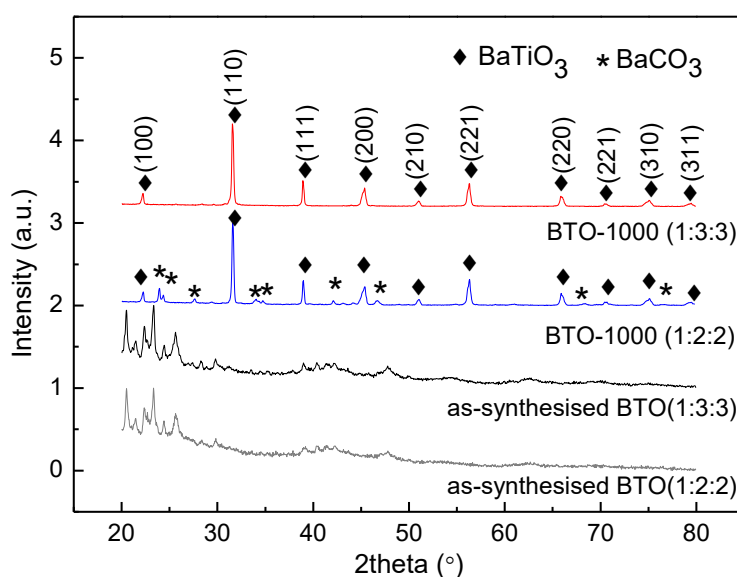


**Figure 1.** XRD patterns of as-synthesised BTOs and BTO-1000 for different molar ratios of Ba:OA:TA, 1:2:2 and 1:3:3

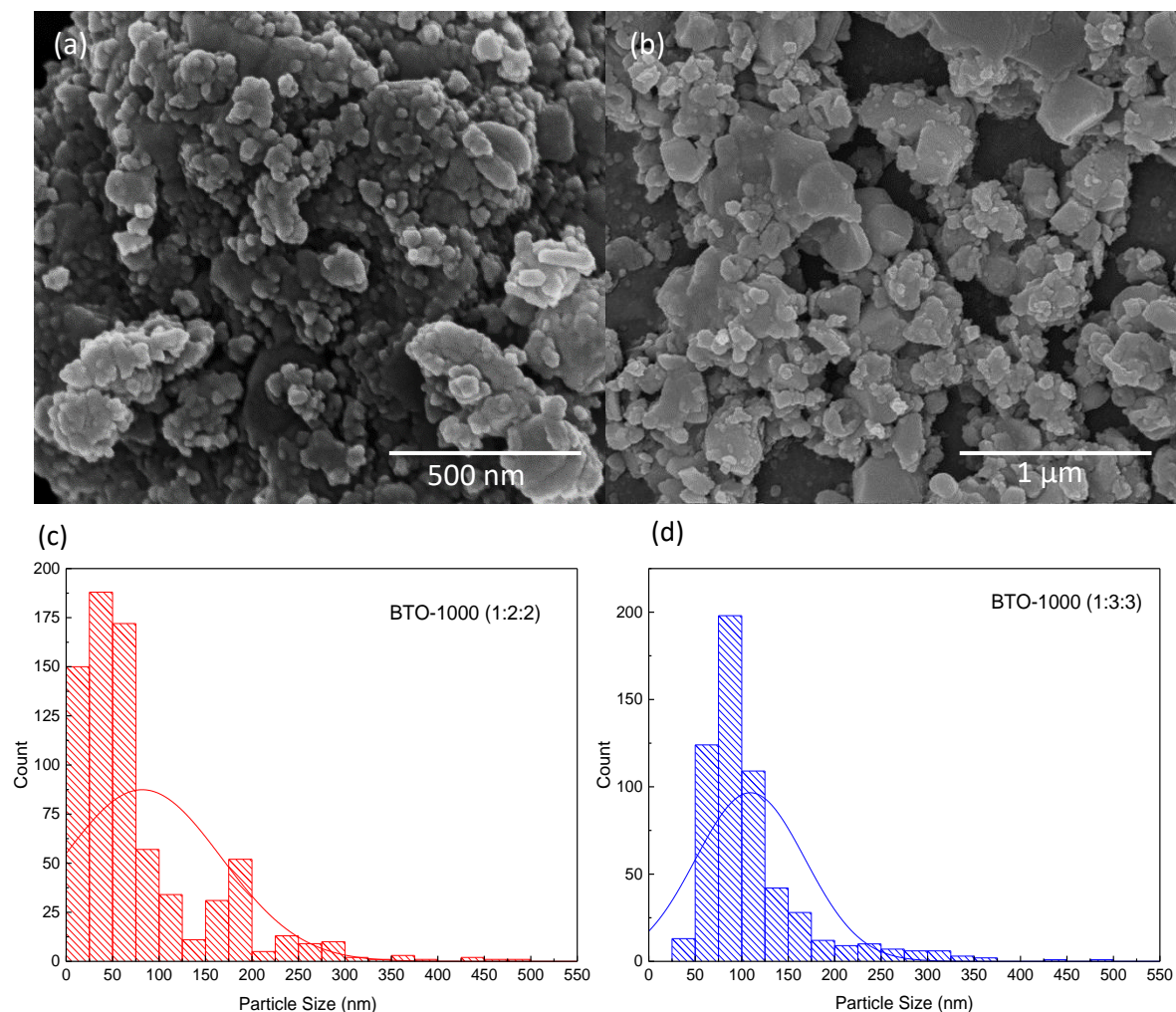


**Figure 2.** FESEM images (a,b) and particle size distributions (c,d) of BTO-1000 (1:2:2) and BTO-1000 (1:3:3).

Oleic acid is crucial to act as capping agent to regulate the shape of BTO in ordered aggregates [11]. It does not absorb or attach well on the {100} facets of BTO nucleic. It also fails to create a confined cubic growth by suppressing the growth of {110} planes. Hence, the BTOs tend to grow into pseudo-ellipsoid shape due to the comparable energy across all the crystallographic planes. The hydrophobic force between oleic acid and BTO nucleic is relatively low as well and thus no self-assembly process is stimulated, unlike BTO (1:8:8) nanocubes reported by Hasbullah *et al.*, (2019) [7].

Figure 3 shows TGA of the as-synthesized BTO (1:2:2) and (1:3:3) with the heating rate of 20°C/min. There were five stages with apparent weight loss at temperatures of 90.6 °C, 261.0 °C, 471.1 °C, 615.6 °C and 781.8 °C. The first stage of weight loss was due to the evaporation of moisture of the as-synthesized BTO and ethanol. Then, the second stage of weight loss showed the decomposition of C<sub>6</sub>H<sub>18</sub>N<sub>2</sub>O<sub>8</sub>Ti forming hydrolyzed Ti species, Ti(OH)<sub>4</sub> and ammonium lactate,

C<sub>3</sub>H<sub>9</sub>O<sub>3</sub>N [16]. Meanwhile, the third stage was the decomposition of dehydrate oxalate originated from tert-butylamine and oleic acid which has been incorporated with the hydrolyzed Ti species and airborne CO<sub>2</sub> into intermediate Ba-Ti-oxycarbonate, Ba<sub>2</sub>Ti<sub>2</sub>O<sub>5</sub>CO<sub>3</sub> metastable phase. The combustion of the major Ba<sub>2</sub>Ti<sub>2</sub>O<sub>5</sub>CO<sub>3</sub> phase and the formation of BaCO<sub>3</sub> and BaTiO<sub>3</sub> phases occurred at 615.89 °C and 781.8 °C. These results were consistent with the co-presence of BaCO<sub>3</sub> phase in the as-synthesized BTO (1:8:8) calcined at 600°C and 700°C [7]. The as-synthesized BTO (1:3:3) exhibited a similar weight loss curve as the as-synthesized BTO (1:2:2) except its third and fourth weight losses happened at lower temperatures of 366.2°C and 462.3°C. As such, the weight losses were associated to the dehydration and decomposition of Ba<sub>2</sub>Ti<sub>2</sub>O<sub>5</sub>CO<sub>3</sub> metastable phase. Above 619.8 °C, no traceable weight loss was observed in the as-synthesized BTO (1:3:3). This result was ascribed to the formation of BaTiO<sub>3</sub> phase without any trace of BaCO<sub>3</sub> as all the residual organic matters had been decomposed completely.

Based on the TGA plot, the overall reaction for the formation of BaTiO<sub>3</sub> with marginal trace of BaCO<sub>3</sub> can be tracked from the reaction between tert-butylamine and oleic acid, hydrolysis of C<sub>6</sub>H<sub>18</sub>N<sub>2</sub>O<sub>8</sub>Ti during hydrothermal synthesis and combustion of intermediate Ba<sub>2</sub>Ti<sub>2</sub>O<sub>5</sub>CO<sub>3</sub> metastable phase. Tert-butylamine reacts with oleic acid with the following deprotonated process:



The hydrolyzed Ti species can react with other C<sub>6</sub>H<sub>18</sub>N<sub>2</sub>O<sub>8</sub>Ti molecules or hydrolyzed species as expressed in Eq. 3 and Eq. 4. The barium species as well as the airborne CO<sub>2</sub> can incorporate into hydrolyzed Ti molecules to form Ba<sub>2</sub>Ti<sub>2</sub>O<sub>5</sub>CO<sub>3</sub> metastable cross-linked phase. The irregular morphology of BTO nanoparticles in this work originated from both the incomplete hydrolysis of C<sub>6</sub>H<sub>18</sub>N<sub>2</sub>O<sub>8</sub>Ti and deprotonating of oleic acid.

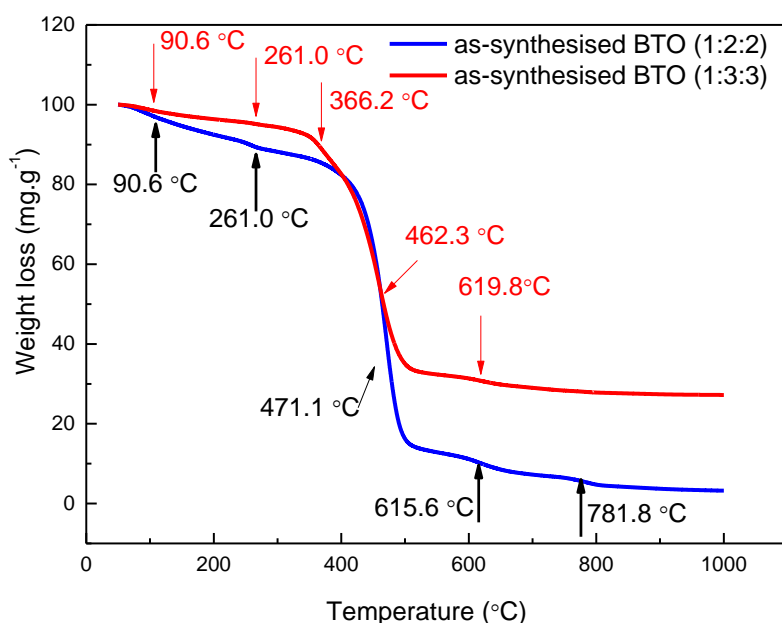


**Figure 3.** TGA curves of as-synthesised BTO (1:2:2) and (1:3:3).

This deprotonated process of oleic acid can improve the connection with barium ion. This process is pivotal for controlling the shape of BaTiO<sub>3</sub> nanostructures [3], particularly to form BaTiO<sub>3</sub> nanocubes [7]. On the other hand, Ti precursor is formed from the hydrolysis of C<sub>6</sub>H<sub>18</sub>N<sub>2</sub>O<sub>8</sub>Ti under hydrothermal conditions. Its initial hydrolysis processes are as follows, where the C<sub>3</sub>H<sub>8</sub>O<sub>3</sub>N component is represented as X:

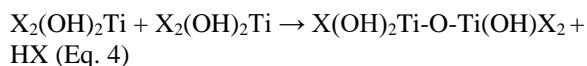
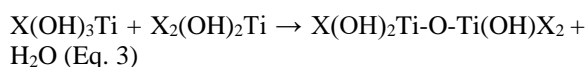
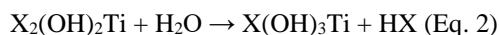
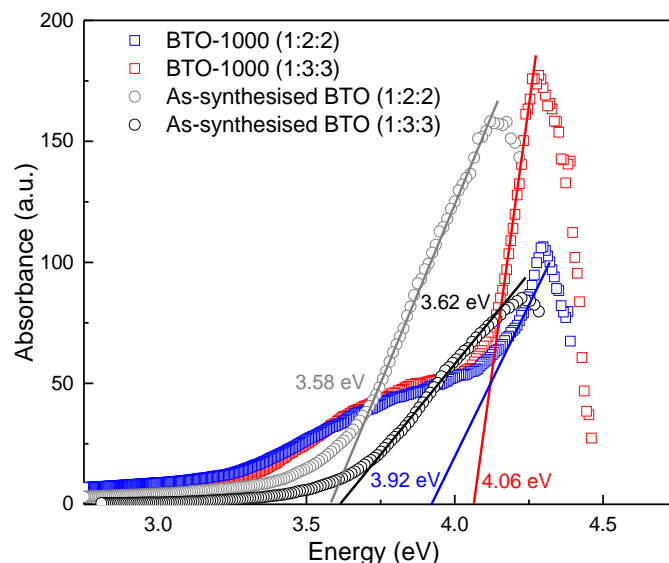


Figure 4 depicts the UV–Vis absorption spectra of the BTO-1000s with well-defined direct band gap energy. The optical band gap,  $E_g$  was estimated from the UV–Vis spectra based on the Tauc and Davis-Mott models [17] with a direct allowed electronic transition. The  $E_g$  of BTOs was determined from the interception of the linear portion of the Tauc plots. The band gaps of BTO-1000 (1:2:2) and BTO-1000 (1:3:3) were 3.95 eV and 4.09 eV, respectively. These  $E_g$  values were higher than that of the reported BTO bulks (2.9–3.4 eV) [5]. The enhancement of the  $E_g$  of BTO-1000s was owed to their high crystallinity upon calcination. Unlike the disordered amorphous BTO, the crystalline BTO exhibits a higher band gap according to the first principle calculation [18]. However, the Urbach tails (exponential decay tail) in the lowest energy edge of the Tauc plots for the BTO-1000s demonstrated that the band structures of the BTO-1000s were non-uniform with the coexistence of localized state [18].



**Figure 4.** Tauc plots of as-synthesised BTOs and BTO-1000 for different molar ratios of Ba:OA:TA, 1:2:2 and 1:3:3

The UV-Vis results are interrelated to photoluminescence spectra. Luminescence is observed when BTO is excited by photo-radiation above the band gap energy. A direct transition from the near conduction band edge to the valence band is permitted if the excitation energy is higher than the band gap. Improving the structural disorder of BTOs by thermal treatment also uplifts the band gap but vanishes their photoluminescence intensities [6, 18]. The photoluminescent emission spectra of BTO-1000s, irradiated and excited at 325 nm (3.81 eV) are shown in Figure 5. Strong violet photoluminescence emissions centred at approximately 434 nm (2.85 eV) were obtained in BTO-1000 (1:2:2) and BTO-1000 (1:3:3). The photoluminescence intensity of the BTO-1000s contrarily reached their highest values as compared to their as-synthesised counter parts. As a result of the excitation used in this work, which was

lower than the obtained band gaps of the BTO-1000s, it was difficult for an electron in the valence band to be effortlessly excited to the conduction band. In turn, it was likely to be excited to the localized levels within the forbidden gap of BTO. Such a photoluminescence increment in the BTO-1000s is imputed to the coexistence of localized state. Consequently, it was evident that both the violet photoluminescence and UV-Vis Urbach effect just below the free exciton energy of the BTO-1000s were in accord with the presence of localized state. Therefore, the recombination of an excited electron in Ti-3d band and hole in the O-2p valence band instigated photoluminescence easily. The localized state could be formed due to structural disorder such as low crystallinity, amorphous state, oxygen vacancies, lattice defects, impurities and local bond dangling [19].

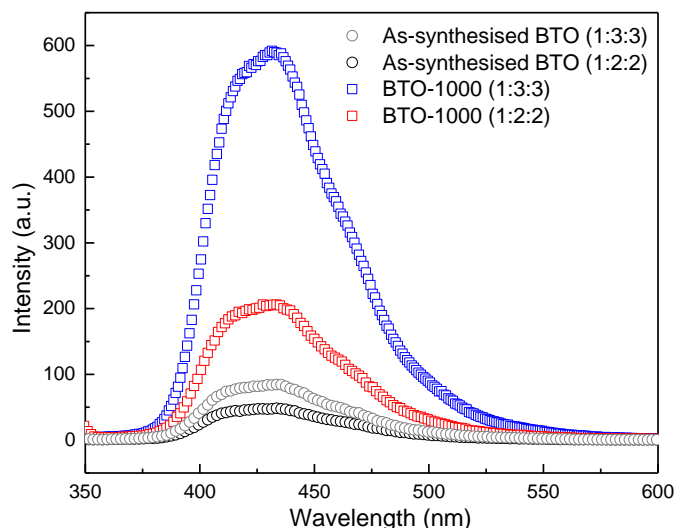


**Figure 5.** Photoluminescence spectra of as-synthesised BTOs and BTO-1000 for different molar ratios of Ba:OA:TA, 1:2:2 and 1:3:3

Based on Souza *et al.* (2012) [20], the strong violet emission in the BTO-1000s stemmed from shallow defects such as oxygen vacancies. The deep defects due to charge carriers trapping, in contrast, emit photoluminescence beyond green, yellow and red emissions. Since the calcination of BTO-1000s was carried in ambient air, the insufficient flow of oxygen during calcination caused oxygen deficiency in the structure of the BTO-1000s [7]. Hence, the density of non-bridging oxygen was higher in the BTO-1000s. These oxygen vacancies not only distorted the BTO-1000 structures but introduced localized electronic states. The oxygen vacancies can act as radiative centres in luminescence process whereas the formation of Ti<sup>3+</sup> can trap the excitons and behave as recombination centres. They trapped electrons from the valance band by creating self-trapping excitons. Thus, oxygen vacancies promote high photoluminescence intensity in BTO-1000s with sufficient excitation (excitation energy < band gap energy) [7].

Apart from the oxygen vacancy, the marginal amount of BaCO<sub>3</sub> phase may influence the photoluminescent behaviour in the BTO-1000s. The photoluminescence intensity of BTO-1000 (1:3:3) was much lower than BTO-1000 (1:2:2) though both of the BTO-1000s underwent the similar calcination condition. This means that surface state also played a pivotal role in the photoluminescence features in the BTO-1000s. The different proportions of Ba: TA: OA was initially to control the growth of BTO-1000 nanostructures with uniform size and morphology. It is worth to note that the ordered aggregates of nanostructures vanish when the proportion is less than 1:8:8 [21]. However, these proportions affect the phase formation of BTO with and without the BaCO<sub>3</sub> secondary phase. Although BaCO<sub>3</sub> does not demonstrate photoluminescent behaviour as explained by Moreira *et al.* (2008) [22] and Orhan *et al.* (2005) [6], the BaCO<sub>3</sub> phase distorted the crystal structure of BTO-1000 (1:2:2). This distortion perturbed the charge transfer from a Ti<sup>3+</sup> ion to a neighbouring O<sup>2-</sup> ion and enhanced the photoluminescence intensity. Surface state excitons are closely related to a high density of unsaturated atoms and dangling bond existing in the periphery of the BTO and BaCO<sub>3</sub> phases found in BTO-1000 (1:2:2). Hence, this indicates that surface state and structural disorder share equal dominant factors for improving the photoluminescence at violet wavelength.

### CONCLUSION

In summary, we demonstrated the synthesis of BTO nanostructures via a hydrothermal method with the assistance of additive, surfactant and heat treatment. BTO-1000 (1:2:2) showed stronger emission than BTO-1000 (1:3:3) in a similar violet wavelength region. The enhanced photoluminescence intensities of the BTO-1000s stemmed from localized state which was evidenced from the tunable optical band gaps and the Urbach effect just below the free exciton energy. These localized states are closely related to oxygen

vacancies. Structural disorder and surface state both were the key factors for improving the photoluminescence of BTO-1000 (1:2:2), which was not completely freed from the BaCO<sub>3</sub> phase.

### ACKNOWLEDGEMENT

This research was supported by the Ministry of Education Malaysia under the Research Acculturation Grant Scheme (RAGS) no.: 57113 and MyMaster scholarship. Authors are gratefully for the financial support from Universiti Putra Malaysia via Putra Grant no.: GP-I/20179552300. These contributions are gratefully acknowledged.

### REFERENCES

1. Mimura, K.-i. and K. Kato (2014) Enhanced dielectric properties of BaTiO<sub>3</sub> nanocube assembled film in metal-insulator-metal capacitor structure, *Applied Physics Express*, **7(6)**, 061501.
2. Song, K., Ma, N., Mishra, Y. K., Adelung, R. and Yang, Y. (2019) Achieving light-induced ultrahigh pyroelectric charge density toward self-powered UV light detection, *Advanced Electronic Materials*, **5(1)**, 1800413.
3. Kato, K., Dang, F., Mimura, K.-i., Kinemuchi, Y., Imai, H., Wada, S., Osada, M., Haneda, H. and Kuwabara, M. (2014) Nano-sized cube-shaped single crystalline oxides and their potentials; composition, assembly and functions, *Advanced Powder Technology*, **25(5)**, 1401-1414.
4. Lee, O., Kursumovic, A., Bi, Z., Tsai, C. F., Wang, H. and MacManus-Driscoll, J. L. (2017) Giant enhancement of polarization and strong improvement of retention in epitaxial Ba<sub>0.6</sub> Sr<sub>0.4</sub> TiO<sub>3</sub>-based nanocomposites, *Advanced Materials Interfaces*, **4(15)**, 1700336.
5. Requena, S., Lacoul, S. and Strzhemechny, Y. (2014) Luminescent properties of surface functionalized BaTiO<sub>3</sub> embedded in poly (methyl methacrylate), *Materials*, **7(1)**, 471-483.
6. Orhan, E., Varela, J. A., Zenatti, A., Gurgel, M., Pontes, F., Leite, E., Longo, E., Pizani, P., Beltran, A. and Andres, J. (2005) Room-temperature photoluminescence of BaTiO<sub>3</sub>: joint experimental and theoretical study, *Physical Review B*, **71(8)**, 085113.
7. Hasbullah, N. N., Chen, S. K., Tan, K. B., Talib, Z. A., Liew, J. Y. C. and Lee, O. J. (2019) Photoluminescence activity of BaTiO<sub>3</sub> nanocubes via facile hydrothermal synthesis, *Journal of Materials Science: Materials in Electronics*, **30(5)**, 5149-5157.
8. Li, H., Huang, S., Zhang, W. and Pan, W. (2013)

- Visible photoluminescence from amorphous barium titanate nanofibers, *Journal of Alloys and Compounds*, **551**, 131-135.
9. Lu, S., Xu, Z., Chen, Mak, C., Wong, K., Li, K. and Cheah, K. (2006) Time-resolved photoluminescence of barium titanate ultrafine powders, *Journal of Applied Physics*, **99(6)**, 064103.
  10. Zhan, H., Jiang, X., Zhu, M., Li, X., Luo, Z. and Shu, K. (2016) Photoluminescence activity of BaTiO<sub>3</sub> nanocrystals dependence on the structural evolution, *Journal of Crystal Growth*, **433**, 80-85.
  11. Itasaka, H., Mimura, K. -I. and Kato, K. (2018) Extra surfactant-assisted self-assembly of highly ordered monolayers of BaTiO<sub>3</sub> nanocubes at the air–water interface, *Nanomaterials*, **8(9)**, 739.
  12. Hasbullah, N. N., Lee, O. J., Chyi, J. L. Y., Chen, S. K. and Talib, Z. A. (2017) Synthesis of BaTiO<sub>3</sub> nanoparticles via hydrothermal method, *Solid State Phenomena*, **268**, 172-176.
  13. Zhu, X., Zhu, J., Zhou, S., Liu, Z., Ming, N. and Hesse, D. (2005) BaTiO<sub>3</sub> nanocrystals: Hydrothermal synthesis and structural characterization, *Journal of crystal growth*, **283(3-4)**, 553-562.
  14. Adireddy, S., Lin, C., Cao, B., Zhou, W. and Caruntu, G. (2010) Solution-based growth of monodisperse cube-like BaTiO<sub>3</sub> colloidal nanocrystals, *Chemistry of Materials*, **22(6)**, 1946-1948.
  15. Dang, F., Mimura, K., Kato, K., Imai, H., Wada, S., Haneda, H. and Kuwabara, M. (2012) In situ growth BaTiO<sub>3</sub> nanocubes and their superlattice from an aqueous process, *Nanoscale*, **4(4)**, 1344-1349.
  16. Bera, J. and Sarkar, D. (2003) Formation of BaTiO<sub>3</sub> from barium oxalate and TiO<sub>2</sub>, *Journal of electroceramics*, **11(3)**, 131-137.
  17. Li, X., Zhu, H., Wei, J., Wang, K., Xu, E., Li, Z. and Wu, D. (2009) Determination of band gaps of self-assembled carbon nanotube films using Tauc/Davis–Mott model, *Applied Physics A*, **97(2)**, 341-344.
  18. Pontes, F., Pinheiro, C., Longo, E., Leite, E., De Lazaro, S. Magnani, R., Pizani, P., Boschi, T. and Lanciotti, F. (2003) Theoretical and experimental study on the photoluminescence in BaTiO<sub>3</sub> amorphous thin films prepared by the chemical route, *Journal of Luminescence*, **104(3)**, 175-185.
  19. Zhang, W., Yin, Z., Zhang, M., Du, Z. and Chen, W. (1999) Roles of defects and grain sizes in photoluminescence of nanocrystalline SrTiO<sub>3</sub>, *Journal of Physics: Condensed Matter*, **11(29)**, 5655-5660.
  20. Souza, A., Santos, G., Barra, B., Macedo Jr, W. Teixeira, S., Santos, C., Senos, A., Amaral, L. and Longo, E. (2012) Photoluminescence of SrTiO<sub>3</sub>: Influence of particle size and morphology, *Crystal Growth & Design*, **12(11)**, 5671-5679.
  21. Ma, Q., Mimura, K. -i. and Kato, K. (2014) Diversity in size of barium titanate nanocubes synthesized by a hydrothermal method using an aqueous Ti compound, *CrystEngComm*, **16(36)**, 8398-8405.
  22. Moreira, M., Mambri, G., Volanti, D., Leite, E., Orlandi, M., Pizani, P., Mastelaro, V., Paiva-Santos, C., Longo, E. and Varela, J. A. (2008) Hydrothermal microwave: a new route to obtain photoluminescent crystalline BaTiO<sub>3</sub> nanoparticles, *Chemistry of Materials*, **20(16)**, 5381-5387.